Nanoscale

Exploring the chelation-based plant strategy for iron oxide nanoparticle uptake in garden cress (*Lepidium sativum*) using magnetic particle spectrometry

Journal:	*Nanoscale*
Manuscript ID	NR-ART-06-2019-005477.R1
Article Type:	Paper
Date Submitted by the Author:	16-Aug-2019
Complete List of Authors:	Ju, Minseon; Case Western Reserve University, Chemistry Navarreto-Lugo, Monica ; Case Western Reserve University, Chemistry Wickramasinghe, Sameera; Case Western Reserve University, Chemistry Milbrandt, Nathalie; Case Western Reserve University, Chemistry McWhorter, Ariel; Case Western Reserve University, Chemistry Samia, Anna Cristina; Case Western Reserve University, Chemistry

ARTICLE

Exploring the chelation-based plant strategy for iron oxide nanoparticle uptake in garden cress *(Lepidium sativum)* using magnetic particle spectrometry†

Received 00th January 20xx,
Accepted 00th January 20xx

DOI: 10.1039/x0xx00000x

Minseon Ju,‡ Monica Navarreto-Lugo,‡ Sameera Wickramasinghe, Nathalie B. Milbrandt, Ariel McWhorter, and Anna Cristina S. Samia*

Although iron is one of Earth's most abundant elements, its availability to plants remains an agricultural challenge, particularly in high pH environments. At high pH, iron forms insoluble ferric oxide-hydroxides that makes it inaccessible to plants. It is estimated that 30% of the world's cropland is too alkaline for optimal plant growth. Staple crops, like rice, are particularly susceptible to iron deficiency, thereby, necessitating the need for continued research in developing iron-based fertilizers. Recent studies have demonstrated the potential of using iron oxide nanoparticles (IONPs) as fertilizers to address iron deficiency in plants, but studies have generated conflicting results. One of the major challenges associated in investigating IONP plant uptake and translocation is the inability to distinguish between intact IONPs versus leached iron ions. In this study, we utilized a new approach based on magnetic particle spectrometry (MPS) to monitor the uptake and distribution of different sized (10 and 20 nm) chelated IONPs in plants. We exposed garden cress (*Lepidium sativum*) plants to EDTA-capped IONPs and observed an 8-fold enhancement in total biomass and 1.4 times increase in chlorophyll production compared to plants treated with a commercial chelated iron fertilizer (Fe-EDTA). Moreover, we demonstrated that the uptake and tissue distribution of IONPs can be quantitatively monitored using MPS, and the results of the analysis were validated by atomic absorption spectroscopy, which is the conventional method used to study IONP plant uptake. Our study demonstrates that MPS is a reliable, sensitive, and effective analytical tool for the development of IONP-based fertilizers.

Introduction

The use of fertilizers to support plant growth accounts for 50 % of global food production.[1] With the current world population exceeding 7.7 billion people and continuing to grow, there is an urgent need for innovations in agriculture for worldwide food supply sustainability.[2] To date, the remediation of iron deficiency in crops remains one of the biggest agronomic challenges.[3,4] Even though iron is regarded as the fourth most abundant element in the Earth's crust, it's availability is highly restricted for plants grown in aerobic soils with neutral to basic pH.[5] In alkaline soils, iron forms insoluble ferric oxide-hydroxides making it unavailable for plant uptake.[6] It is estimated that about 30 % of the world's cropland is too basic for optimal plant growth, and iron deficiency becomes a major constraint for crop yield, which can ultimately affect the health of people whose diet relies on plant food sources.[7,8] In particular, staple crops like rice are susceptible to iron deficiency, thereby requiring the need for continued research in developing effective iron sources that will enable sustainable fertilizer management.[9]

In plants, iron deficiency leads to chlorosis, a condition that is visibly manifested in the yellowing of leaf tissue due to reduced chlorophyll production.[10] If left untreated, chlorosis can lead to slowed plant growth, reduced biomass, and eventual plant death.[11] In order to cope with iron deficiency, plants have developed two main strategies for the effective uptake of iron: a reduction-based strategy, and a chelation-based strategy.[12,13] These mechanisms have facilitated the transport of iron, but also promoted iron overload leading to adverse effects.[14] In the reduction-based strategy, the first step involves the acidification of the root environment (rhizosphere) to increase the amount of available Fe(III), which involves the H^+-translocating P-type ATPase AHA2.[15] Subsequently, Fe(III) is reduced to Fe(II) by the root surface-localized ferric reductase oxidase2 (FRO2) enzyme prior to its uptake by the iron-regulated transporter 1 (IRT1) protein that is found in the epidermal cells;[16,17] IRT1 is a Fe(II) transporter protein that ultimately facilitates iron uptake in plants.[18] The problem associated with this pathway is that the broad specificity of IRT1 also promotes the transport of other divalent cations such as zinc, manganese, cobalt, and cadmium that could be present in the plant growth medium, thereby

Department of Chemistry, Case Western Reserve University, 10900 Euclid Ave., Cleveland, OH 44106, USA.
Email: anna.samia@case.edu; Tel: +1-216-368-3852
†Electronic Supplementary Information (ESI) available: See DOI: 10.1039/x0xx00000x
‡ Denotes equal author contributions.

competing with the absorption of iron.[19–21] Conversely, in the chelation-based strategy, the plant releases phytosiderophores (PS) in the roots, which form stable Fe-PS chelates. These chelates can then be transported across the root plasma membrane through the yellow stripe-like (YSL) family of transporter proteins found on the root surface. PS are hexadentate ligands with amino and carboxyl groups that form Fe(III) coordination complexes.[22] While these two pathways have facilitated the iron uptake process in plants, a significant amount of cultivated soils still suffer from low iron availability, which force agronomists to use fertilizers as the standard approach to treat lime-induced chlorosis.[23] This brings new challenges due to improper or over application of fertilizers that under aerobic conditions promote the formation of reactive oxygen species (ROS) as by-products of Fenton reactions, which damage vital plant cellular components.[24,25] To address this problem, the use of chelated iron fertilizers to treat chlorosis has been adapted in the field to promote iron bioavailability to plants. Studies have shown that chelated iron fertilizers like Fe-EDTA (ethylenediaminetetraacetic acid) remain available for longer periods than non-chelated iron analogs.[8,26] Alternatively, recent studies have demonstrated the potential of using iron oxide nanoparticles (IONPs) as fertilizers to address iron deficiency in plants.[27] However, while some studies demonstrate significant enhancement in plant growth upon treatment with IONPs,[28-31] other investigations provide conflicting results.[32,33] This phenomenon can be largely attributed to the wide variations in experimental parameters pertaining to IONP size, shape, surface coating, plant type, and growth conditions.[32,,34–36]

In order for IONP-based fertilizers to reach their full potential, it is necessary to address key materials design parameters for optimal plant uptake. This includes optimization of nanoparticle size to facilitate passage in plant tissues, and suitable surface coating to ensure particle stability against aggregation. To address these challenges, we have developed a synthetic approach to produce highly stable IONPs that mimic the chelating ligands found in commercial iron fertilizers. By adapting an EDTA-terminated silane ligand as surface coating, we were able to promote effective plant root accumulation and plant uptake of the IONPs and the sustainable release of nutritional iron from the IONPs in the different plant tissues. Moreover, we have effectively demonstrated that the plant root accumulation and plant uptake process and IONP translocation in different plant tissues can be effectively monitored using magnetic particle spectrometry (MPS), a new magnetic relaxometry analytical method that is used to characterize the magnetic behaviour of IONP based imaging tracers.[37-44] Currently, IONP plant uptake and translocation studies have utilized atomic absorption spectroscopy (AAS) and electron microscopic methods to study the fate of this nanomaterial in the complex biological matrix of plant systems.[45] However, these methods lack the ability to simultaneously detect and quantify IONPs in a non-destructive manner. AAS involves laborious strong acid digestion sample processing, and it still unable to distinguish between intact IONPs versus leached iron ions uptaken by the plants.[45] While electron microscopic techniques such as transmission electron microscopy (TEM) and scanning electron microscopy (SEM) can confirm the translocation of IONPs to aerial components and identify changes in the morphology of the material caused by the process, however, it requires an extensive and expensive sample preparation process that also uses toxic chemicals.[46] Electron microscopy techniques also lack the ability to quantify the total amount of IONPs uptaken in plant tissues. In this study, we demonstrate that the plant root accumulation and plant uptake process and translocation of IONPs can be efficiently monitored using MPS. This approach serves as an important contribution in the field as it facilitates the ability to monitor the biotransformation and the fate of magnetic nanomaterials inside biological systems. In this report, we present the use of MPS to monitor the absorption and translocation of different sized (10 nm and 20 nm) EDTA-coated iron oxide nanoparticles ($IONP_{10}$-EDTA and $IONP_{20}$-EDTA) in garden cress (*Lepidium sativum*) plants. Garden cress was selected as a model plant system in this study because of its short growth cycle and its nutritional value. Non-grass plant species like the garden cress plant (*Lepidium sativum*) used in our study, which is a close relative to the more commonly investigated mouse-ear cress plant (*Arabidopsis thaliana*), have been shown to contain YSL transporter proteins that are responsible for transporting metals complexed by nicotianamine (NA), an iron chelator that is structurally similar to PS that is found in all higher plants. [17, 22,47] We evaluated the IONP-EDTA effect on plant biomass, growth, and chlorophyll production, in comparison to effects of plant exposure with a commercial Fe-EDTA fertilizer. Our MPS studies were validated by AAS and TEM, and we demonstrated that this method is reliable, sensitive, and an effective analytical tool for the investigation and development of IONP-based fertilizers.

Results and discussion

Synthesis and characterization of EDTA-functionalized iron oxide nanoparticles

Iron oxide nanoparticles capped with oleic acid (IONP-OA) were synthesized through a thermal decomposition method[48,49] followed by a ligand exchange process with *N*-(trimethoxysilylpropyl)ethylenediaminetriacetate to generate water soluble EDTA-capped iron oxide nanoparticles (IONP-EDTA) as illustrated in Fig. 1a. Transmission electron microscopy (TEM) analyses confirmed that the synthesized nanoparticles are monodisperse with spherical morphologies and median core sizes of 9.9 ± 0.7 nm ($IONP_{10}$-EDTA) and 19.5 ± 1.1 nm ($IONP_{20}$-EDTA), respectively (Fig. 1b). The successful silane-EDTA surface functionalization of the IONPs was verified from the obtained Fourier transform infrared spectra (Fig. 1c). The as-synthesized IONP-OA shows the characteristic metal carboxylate peak at 1639 cm^{-1} and the C-H stretch at 2922 cm^{-1}, which is indicative of the original OA ligand (Fig. 1c). Upon ligand exchange, the identifying Si-O vibrational stretch becomes apparent in the IONP-EDTA sample, reflecting the

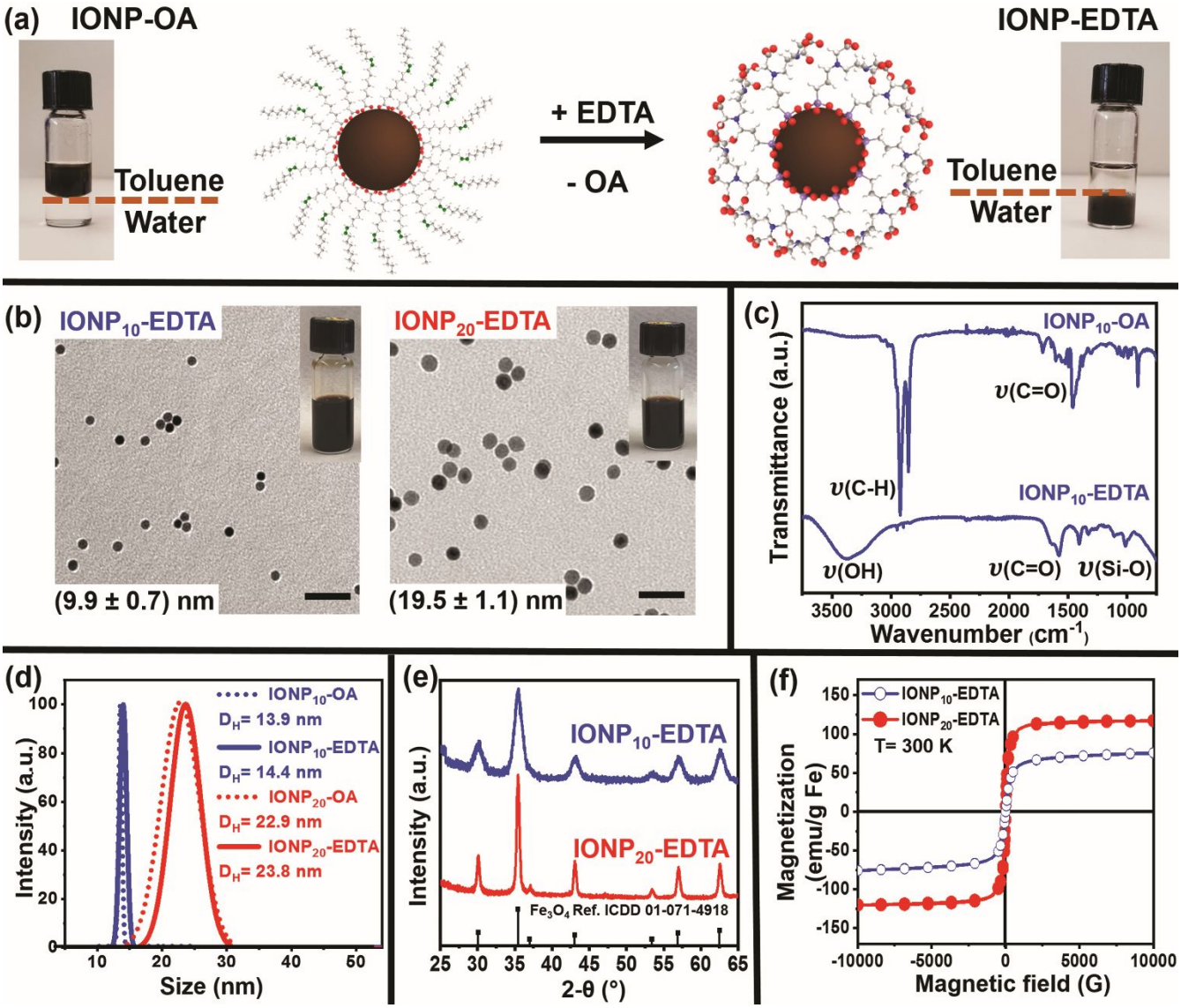

Fig. 1 (a) Schematic diagram of the ligand exchange process to generate water soluble EDTA-capped iron oxide nanoparticles (IONP-EDTA) from as-synthesized oleic acid capped iron oxide nanoparticles (IONP-OA). (b) Transmission electron microscope (TEM) images of EDTA-capped iron oxide nanoparticles with average diameters of 9.9 nm ($IONP_{10}$-EDTA) and 19.5 nm ($IONP_{20}$-EDTA), respectively; the scale bars represent 50 nm. (c) FTIR spectra of a representative IONP-OA and IONP-EDTA sample illustrating the success of the ligand exchange process. (d) Hydrodynamic diameters of the IONP-OA and IONP-EDTA samples measured using dynamic light scattering. (e) Powder x-ray diffraction patterns of the IONP-EDTA samples demonstrating magnetite (Fe_3O_4) crystalline phases. (f) Field-dependent magnetization curves obtained for the IONP-EDTA samples measured at 300 K from 1 T to -1 T using a vibrating sample magnetometer.

effective substitution of OA with the silane-EDTA ligand. Moreover, the presence of the broad absorption band at 3298 cm^{-1} corresponding to the stretching vibration of OH, and the C=O peak around 1651 cm^{-1}, confirm the presence of EDTA on the IONP surface (Fig. 1c). As shown in Fig. 1d, following the ligand exchange process, the hydrodynamic diameters of the fabricated IONP-EDTA samples did not change significantly as evaluated by dynamic light scattering (DLS). Moreover, zeta potential measurements confirm the presence of the negatively charged carboxylate groups on the $IONP_{10}$-EDTA and $IONP_{20}$-EDTA surfaces (Fig. S1[†]). The crystalline phases of the IONP-EDTA samples were investigated using powder x-ray diffractometry (PXRD) and the samples were shown to be that of the magnetite (Fe_3O_4) phase (Fig. 1e). Magnetic measurements performed using a vibrating sample magnetometer (VSM) revealed that both $IONP_{10}$-EDTA and $IONP_{20}$-EDTA are superparamagnetic at room temperature, with higher saturation magnetization for the larger $IONP_{20}$-EDTA sample (Fig. 1f).

Garden cress growth conditions and incubation with IONP-EDTA

To evaluate the effects of IONP-EDTA exposure on the growth and phenotypic traits of plants, garden cress (*Lepidium sativum*) was chosen as a model plant system because of its favourable growth cycle, good nutritional value, and ideal plant biology for research.[50] In our study, groups of 10 seedlings were germinated and grown for 5 days in aqueous

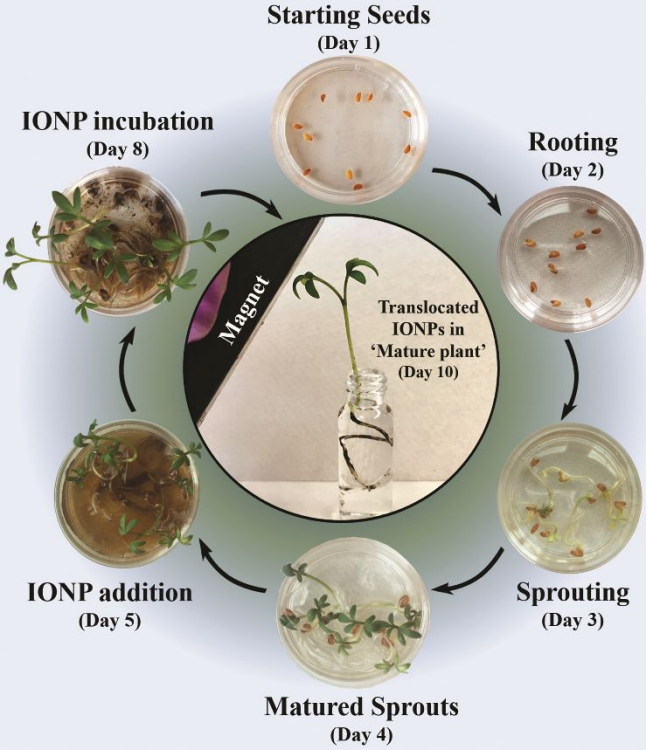

Fig. 2 Growth conditions adapted for the garden cress plants: from seedlings (Day 1) to translocation of IONPs in mature plants (Day 10). The photo at the center is a snapshot of the video provided in the ESI that demonstrates the magnetic attraction of a representative 10-day old plant that was pre-incubated with IONPs to an external bar magnet.

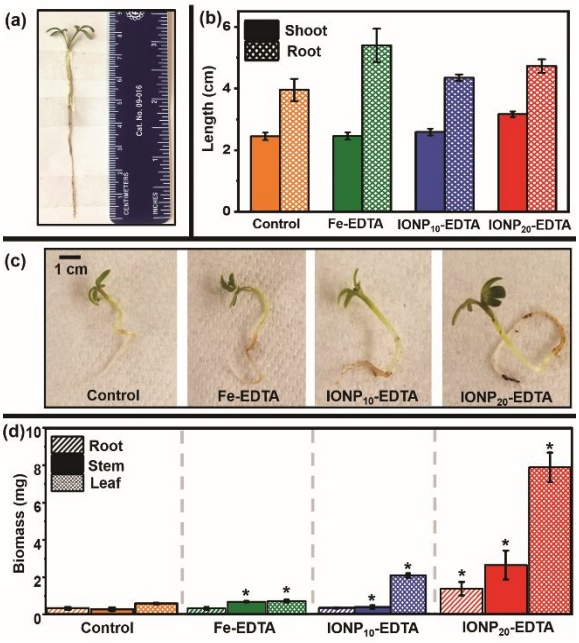

Fig. 3 Phenotypic observations on the effect of a 5-day IONP-EDTA incubation period on garden cress plants: (a) length measurement method; (b) average length measurements (n=50 plants) of the shoot (leaf+stem) and root plant components; (c) representative photographs of the harvested plants exposed to the different treatments; (d) average biomass measurements of the different plant tissues (n=50 plants). An asterisk (*) indicates that the difference in means of the treatments are statistically significant from the control treatment at $p < 0.05$.

media to mimic hydroponic conditions (Fig. 2). The resulting 5-day old matured sprouts were subsequently exposed to different treatment conditions: water (control treatment), commercial Fe-EDTA fertilizer (500 mg/L of Fe), two sizes of EDTA-capped iron oxide nanoparticles ($IONP_{10}$-EDTA and $IONP_{20}$-EDTA each with 500 mg/L of Fe). After 5 days of incubation, sprouts were harvested for investigation. The concentration of Fe (500 mg/L) used in our plant studies was chosen based on previous studies reported by other groups.[28,30,34,35] Additionally, we have performed control experiments comparing the growth of garden cress plants upon exposure to 500 mg/L Fe versus 5000 mg/L Fe using similar growth conditions that we previously reported, which demonstrated that plant growth was retarded at higher Fe-EDTA concentration (Fig. S2†). Moreover, we compared the effect of applying the IONP-EDTA treatment at different stages of the plant growth cycle to evaluate the effect of a 5-day versus 8-day incubation time period (Fig. S3†), and could show that application at day 5 is more favorable for the garden cress plant.

As shown in Fig. 2, the garden cress seeds germinate after 1 day, and by day 5 the seedlings mature into plants with well-defined roots and leaves. At this growth stage, it is suitable for the plants to be incubated with the different treatments since they typically require additional nutrients for healthy growth.[28]

Effect of IONP-EDTA treatment on garden cress length and biomass

The $IONP_{10}$-EDTA and $IONP_{20}$-EDTA garden cress plant treatments were evaluated after 5 days of incubation time and compared with the plant exposure to commercial Fe-EDTA fertilizer. Fig. 3a demonstrates the method used to evaluate the length of the collected garden cress plants, which includes measurement of the entire plant from the leaves to the root tips. Plotted in Fig. 3b are the length measurements obtained from the shoots (leaf+stem) and roots of the garden cress plant samples after 5 days of exposure to the different treatments. The shoot length showed no significant difference among the various treatments ($p<0.05$, $n=50$) even though the $IONP_{20}$-EDTA treated plants appear slightly longer in length (Fig. 3b). Similar results were obtained in comparing the root lengths, with the plants treated with the Fe-EDTA fertilizer showing slightly longer average root length.

On the other hand, comparison of the phenotypic plant traits showed dramatic effects on the resulting plant growth upon exposure to the IONP treatments as shown in Fig 3c. The plants exposed to IONP-EDTA have significantly thicker stems and bigger leaves in comparison to the control plants and the plants treated with the Fe-EDTA fertilizer. These observations were reflected in Fig. 3d, where the biomass measurements showed an 8x fold increase in biomass for those plants treated with $IONP_{20}$-EDTA versus the control or Fe-EDTA fertilizer. The comparable length measurements between garden cress experimental and control groups reflect no significant signs of

toxicity upon $IONP_{10}$-EDTA or $IONP_{20}$-EDTA treatments. The observed biomass increase in plants exposed with IONPs is consistent to what was previously reported by other groups.[28,31] Sheykhbaglou *et al.* and Dhoke *et al*. observed the increase in biomass of soybean and mung plants after their treatments with IONP using a foliar application route. When compared to previous reports, the significantly higher biomass increase observed in our study could be attributed to the application of the treatments under hydroponic growth conditions, which provide continuous and optimum channels for the IONPs to reach the different plant components.[51]

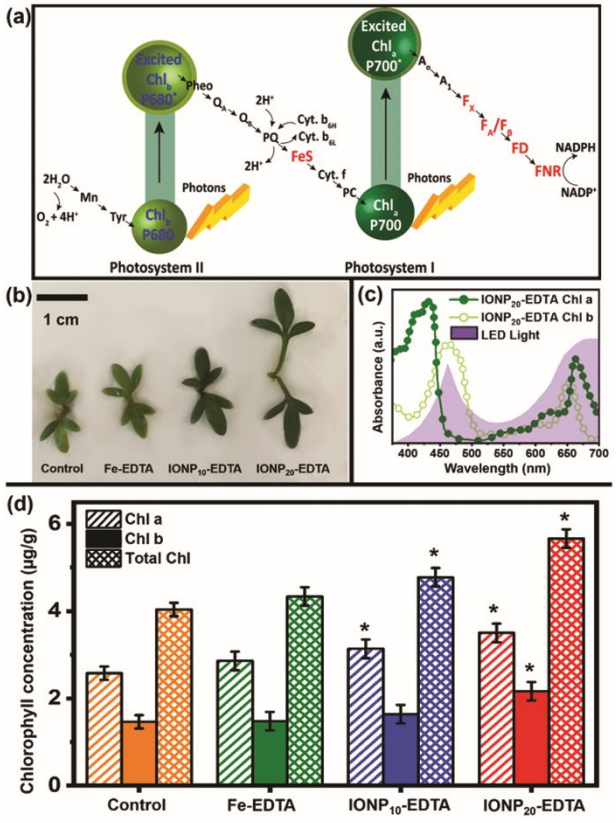

Fig. 4 Effects of IONP-EDTA treatment on chlorophyll production in garden cress plants: (a) schematic representation of the photosynthetic units showcasing the participation of Fe-based electron transport protein complexes indicated in red where, Mn-manganese center; Tyr-tyrosine; Chl_b P680-photosynthetic reaction center of chlorophyll b in photosystem II; Pheo-pheophytin; Q_A and Q_B-plastoquinones; PQ-reduced plastoquinone; FeS-Rieske iron-sulfur protein; Cyt. f-cytochrome f; Cyt. b_{6L} and Cyt. b_{6H}-lower and higher potential cytochrome b_6 molecules, respectively; PC-plastocyanin; Chl_a P700-photosynthetic reaction center of chlorophyll a in photosystem I; A_0-chlorophyll a; A_1-phylloquinone; F_x, F_A, and F_B-iron-sulfur centers; FD- ferredoxin; FNR-ferredoxin NADP oxidoreductase ; (b) images of representative leaves from each treatment group; (c) representative absorption spectra of the Chl_a and Chl_b extracted from treated garden cress plants; (d) effect of the different treatment conditions on the concentration of chlorophyll a, b, and total chlorophyll amounts extracted from the treated garden cress plants. An asterisk (*) indicates that the difference in means of the treatments are statistically significant from the control treatment at $p < 0.05$ with n=30.

Effect of IONP-EDTA treatment in garden cress chlorophyll content

In addition to the increase in biomass, there was also a significant enhancement in chlorophyll (Chl) production observed in the plants treated with IONP-EDTA (Fig. 4). In order for the photosynthetic system to operate, plants need key minerals, such as Fe.[52] At least 80 % of Fe found in plants is located in the leaves, as it is a key component in the electron transfer processes of photosynthesis.[52] Both chlorophyll a (Chl_a) and chlorophyll b (Chl_b) play important roles in photosynthesis by absorbing light with the consequent electron transport that is enabled mostly by Fe-S proteins (Fig. 4a).[53] These Fe-S proteins are composed of Fe-S clusters, and their main function is electron transfer through the Fe^{2+}/Fe^{3+} oxidation states.[54] Fe-S electron transfer and its role in chlorophyll production are the vital steps in the process of production of plant energy, growth, and development.[54] Previous studies reported that a 30 % enhancement in photosynthesis can generate an increase in relative growth of 10 %.[55] This finding was rationalized by the limitations of plants systems to process large amounts of carbohydrates available in short periods of time.[55]

Our studies demonstrated an increased production of chlorophyll in the plants exposed to $IONP_{20}$-EDTA, which is evidenced by the observations in Fig. 4b-d. By extracting chlorophyll (Fig. S4†) and separating its components into Chl_a and Chl_b, higher concentrations of Chl_a relative to Chl_b were measured in plants treated with IONP-EDTA as shown in Fig. 4c-d. Chl_a serves as the primary photosynthetic pigment that promotes plant biomass, while Chl_b is an accessory pigment that collects complementary light energy and transfers to Chl_a (Fig. 4b-d).[53] As Fe plays an important role in these photoprocesses,[52-55] the observed results support the translocation of $IONP_{20}$-EDTA into the garden cress leaves and the sustainable release of Fe for an optimum utilization in the photosynthetic electron transport protein complexes represented in red in Fig. 4a. The sustainable release of Fe from IONP-EDTA, provides a sufficient and continuous supply of Fe to the Fe-based protein complexes that facilitate the electron transfer needed in the production of Chl_a. The increased production in Chl_a subsequently boosts the production of energy and plant growth.[53] These results suggest that $IONP_{20}$-EDTA can promote a significant increase in plant biomass and chlorophyll production by providing continuous amounts of suitable concentrations of Fe.

Nanoparticle uptake in plants has been a controversial topic in agricultural science due to contradictory sets of information about their absorption and translocation in different plant species and under different growth conditions.[32,35,36,38] However, the exploration of IONPs as a potential fertilizer agent for some plant species remains a promising area of study; an idea that is supported by the current observed phenotypic response obtained after incubation of garden cress plants with $IONP_{20}$-EDTA, which is consistent with what other groups have reported in different plant species.[45,46]

Magnetic particle spectrometry (MPS)

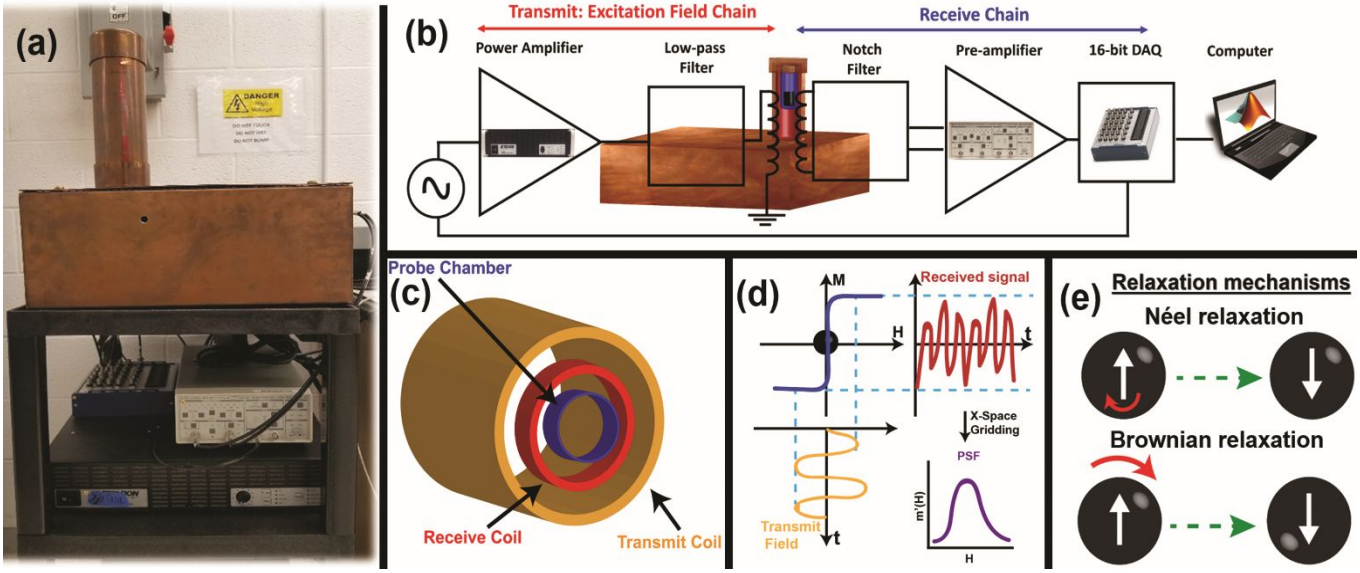

Fig. 5 Schematic representation of the MPS instrument and signal generation process: (a) photograph of the x-space MPS system at Case Western Reserve University; (b-d) MPS instrument components and schematic representation of the point spread function (PSF) signal generation process; (e) magnetic relaxation mechanisms that contribute to the MPS signal.

In this study, MPS was used to monitor the root accumulation and plant uptake and translocation of IONPs in garden cress plants from a hydroponic media. The magnetic particle spectrometer (also known as magnetic particle relaxometer) used for the analysis is a custom x-space magnetic particle relaxometer at Case Western Reserve University as shown in Fig. 5a.[56,57] This relaxometer is a sensitive tabletop system that facilitates the ease of monitoring superparamagnetic IONPs in plant systems with minimal sample preparation. Our work shows the diverse capabilities of MPS analysis to monitor the concentration of IONPs in solution (for the uptake of IONPs from hydroponic media) and also inside plant tissues (for translocation studies). Once the sample aliquot or plant tissue is collected it can be directly measured in the MPS system where the data acquisition and signal reconstruction are conducted using a MATLAB interface software. Shown in Fig. 5b is a schematic representation of the components of our MPS instrument. During measurement, a sinusoidal signal with f_o=16.8 kHz is fed to an audio power amplifier and low-pass filter, which generates a magnetic field amplitude of 20 mT at the sample chamber. The resulting signal from the IONPs is detected by the receive coil, then notch filtered to remove f_o feedthrough. The final sample signal is amplified by a low-noise preamplifier before being sampled at 500 ksps; one sample measurement takes 30 s.[57]

The magnetic particle spectrometer measures the one-dimensional point spread function (PSF) of an IONP.[56,57] The spectrometer generates an excitation field that periodically drives the IONP magnetization into and out of saturation, which is analogous to the field free region (FFR) being swept back-and-forth over the sample under investigation. The field excitation induces a magnetization flip that is detected in the nearby receive coil. The resulting signal from the IONPs is inductively detected and gridded to the (known) instantaneous magnetic field value to generate the PSF (Fig. 5c-d).[41,56-60] Upon exposure to the sinusoidal magnetic field, the IONPs undergo magnetization reversal using a combination of Brownian and Néel relaxation mechanisms as illustrated in Fig. 5e.[61-64]

Magnetic particle spectrometry monitoring of IONP root accumulation and plant uptake

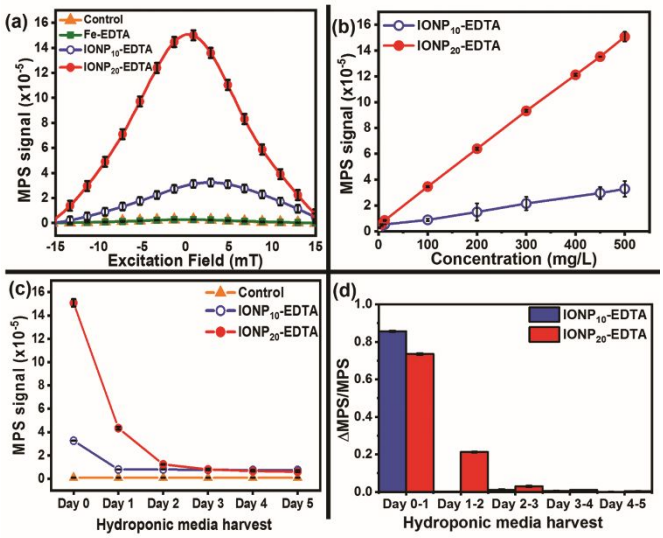

Fig. 6 Monitoring of IONP root accumulation and plant uptake in 5-day old garden cress plants from hydroponic growth media: (a) representative MPS signals of the different plant treatments each containing 500 mg/L Fe with water as control treatment; (b) calibration curves for the $IONP_{10}$-EDTA and $IONP_{20}$-EDTA treatments; (c) MPS monitoring in hydroponic media; (d) daily change in MPS signal for the IONP-EDTA samples in hydroponic media. The error bars were obtained with n= 5.

For the quantification of the total Fe taken up by the plant, the decrease in concentration of the IONP-EDTA samples from the hydroponic growth media was monitored using MPS. To ensure that changes in the MPS signal is not due to IONP-EDTA instability in the hydroponic media, we monitored the PSFs of the $IONP_{10}$-EDTA and $IONP_{20}$-EDTA samples over the span of the 5-day plant incubation period and no considerable changes in MPS signal were observed (Fig. S5†). Representative MPS signals obtained from comparing the PSFs of the different plant treatments, each with a total of 500 mg/L Fe content (water served as the control treatment), is shown in Fig. 6a. The MPS signal obtained from the larger $IONP_{20}$-EDTA sample is higher than that of the smaller $IONP_{10}$-EDTA sample (Fig. 6a-c). This result is consistent with what other groups have previously observed,[41,42] whereby the MPS signal is proportional to the IONP volume that leads to enhanced magnetization with increase in particle size.[62] The PSFs of different concentrations of $IONP_{10}$-EDTA and $IONP_{20}$-EDTA samples were measured to generate the calibration curves shown in Fig. 6b. The calibration curves were used to estimate the amount of IONP that was taken up from the hydroponic media. Results showed that the $IONP_{10}$-EDTA sample was taken up faster in the first 24 h after incubation period. On the other hand, $IONP_{20}$-EDTA showed a continuous removal of the IONP from the growth media throughout the course of the 5 day plant exposure time as shown in Fig. 6c-d. Enlarged versions of Fig.6c-d can be found in the ESI as Fig. S6†.

While the $IONP_{10}$-EDTA sample was taken up faster, the phenotypic effects of enhanced biomass and chlorophyll production were more dramatic for the $IONP_{20}$-EDTA treatment. These observations could be attributed to a more gradual but sustainable source of Fe coming from the larger $IONP_{20}$-EDTA sample, which was consumed over the span of a 4-day incubation period, as compared to the 1-day complete plant root accumulation and plant uptake of the $IONP_{10}$-EDTA sample.

Previous studies have shown that Fe uptake in the rhizosphere can be mediated by ferric reductase defective3 (FRD3), which aides in the exportation of Fe-citrate

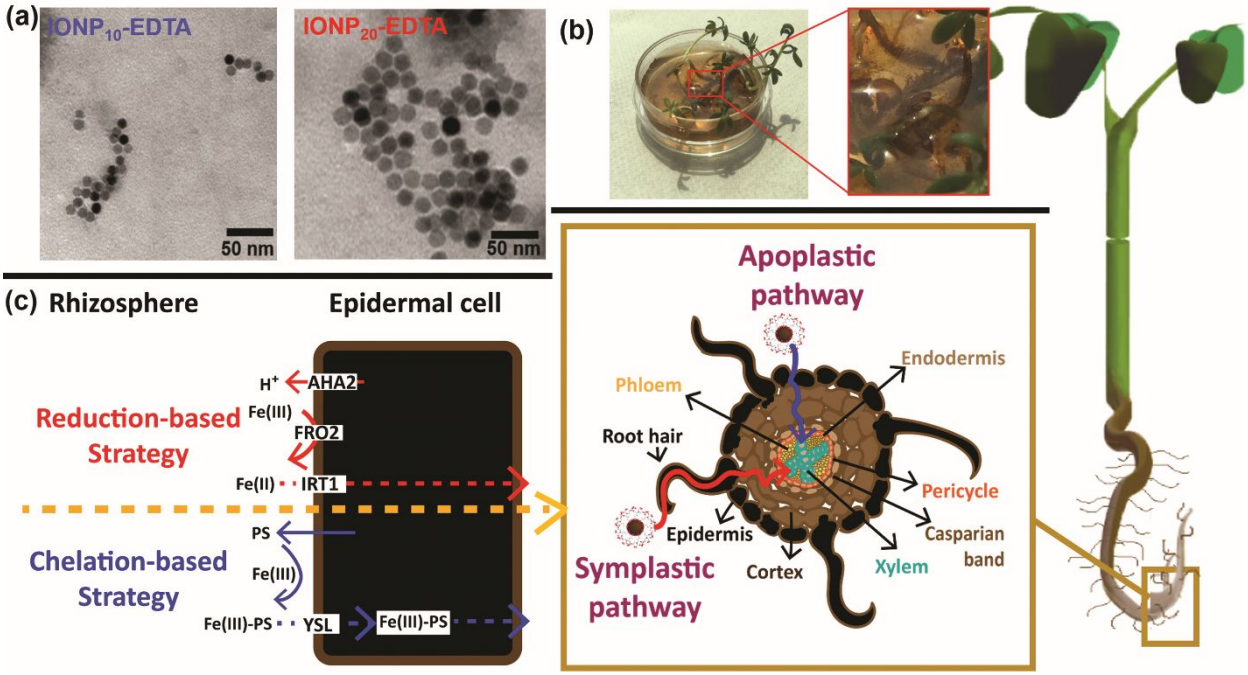

Fig. 7 (a) TEM images of $IONP_{10}$-EDTA and $IONP_{20}$-EDTA after plant incubation in hydroponic growth media. (b) Representative photograph of IONP-EDTA samples concentrating around the root hairs of garden cress after 30 min of incubation. (c) Schematic representation of the pathways for the uptake of Fe through the plant roots.

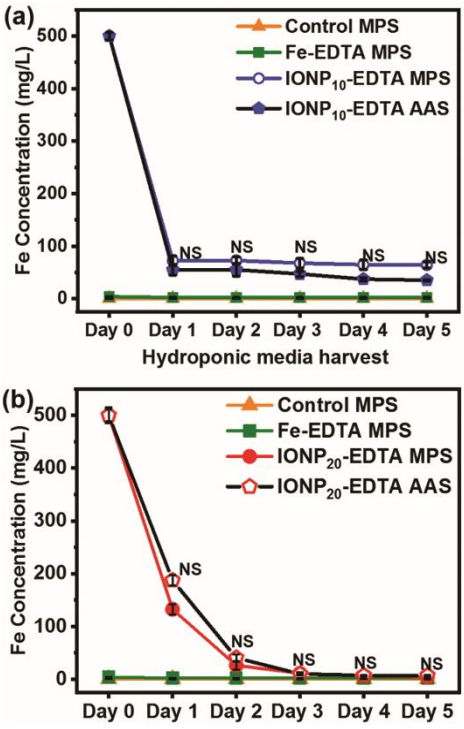

Fig. 8 Comparison and validation of MPS results with atomic absorption spectroscopy (AAS): (a) $IONP_{10}$-EDTA and (b) $IONP_{20}$-EDTA treatments, respectively. The error bars were obtained with n=5. NS indicates that the difference in means of the MPS and AAS measurements are not statistically significant from each other at $p < 0.05$.

complexes into the plant through the xylem.[65] Even if such type of enzymes were released from the rhizosphere of our test plants, we did not see considerable changes in the particle size or morphology of the $IONP_{10}$-EDTA and $IONP_{20}$-EDTA samples remaining in the hydroponic media as shown in the obtained TEM images of the IONPs in Fig. 7a. Fig. 7b shows the IONPs concentrating close to the root hairs after 30 min of incubation in the hydroponic media, which supports an root accumulation and plant uptake strategy for the IONP-EDTA samples through the roots. One of the concerns was the dissolution of the IONPs to cause considerable release of Fe ions before the particles were able to enter the plant. Non-chelated forms of Fe can have toxic effects due to its Fenton reaction by-products,[52] which indicate that the chelation-based strategy is the likely mechanism that the plant has developed for the uptake and translocation of the maximum amount of Fe from the rhizosphere while protecting themselves from the toxic effects of Fe overload[12,13] (Fig. 7c). To exploit the chelation-based strategy, we engineered our IONPs to be surface functionalized with silane-EDTA because of the reported favourability of Fe-EDTA fertilizer uptake in plants. Moreover, the silane anchoring group provides strong coordination for capping the IONP surface thereby providing enhanced protection, and ensuring good dispersity of the IONPs (Fig. S5†). This materials design strategy helps to promote the sustainable release of Fe through the translocation process without the need for multiple fertilizer application. Fig. 7c shows a schematic representation of the root strategies for the uptake of Fe in different oxidation states and the two possible routes for the uptake and translocations of IONP into aerial components (apoplastic and symplastic pathways).[12,13] We hypothesize that EDTA mimics the function of PS to facilitate the transport of the IONP into the plant tissues through the root system. The slower removal of the $IONP_{20}$-EDTA sample from the hydroponic media compared to commercial Fe-EDTA fertilizer (Fig. S7†) could represent an alternative for a more efficient uptake of iron that avoids iron deficiency and/or overload that leads to increase in free electron careers in the plant and the formation of toxic ROS species.[52]

Validation of MPS results with atomic absorption spectroscopy

The MPS calculated concentrations of Fe in the hydroponic media measurements were validated by atomic absorption spectroscopy (AAS) and compared in order to determine the sensitivity of the proposed method. MPS and AAS results showed no significant difference after performing the F-test and Student's T-test analysis, with a 95 % confidence level. The changes in Fe concentration for the $IONP_{10}$-EDTA and $IONP_{20}$-EDTA samples as measured by MPS and by AAS are shown in Fig. 8.

Magnetic particle spectrometry monitoring of IONP translocation

For further exploration of the MPS analytical capabilities, the sensitivity of the method was evaluated by measuring the magnetization response of the translocated IONPs in the leaves, stem, and root components of the garden cress plants

(Fig. 9a). To check the contribution of Brownian relaxation on the MPS signal upon the root accumulation and plant uptake of the IONP-EDTA in the plant tissues, we compared the signal of the samples in different matrices (Fig. S8†). The 3 % agarose gel matrix utilized in the study has an average pore size[66] that should represent the typical pore sizes found in different plant tissues.[67] In our study, we did not observed any significant decrease in the MPS signal upon comparing the data obtained in hydroponic versus 3% gel matrix. The signal obtained from the MPS measurements of the plant tissues were used in conjunction with the previously obtained calibration curves to determine the concentration of Fe in each plant component. The results were compared with the total Fe concentration obtained by AAS analysis. Both techniques showed higher concentrations of Fe in the roots, followed by the leaves, and less in the stems as shown in Fig. 9b. These data support the results obtained from the hydroponic media MPS analysis that predicted absorption of intact nanoparticles in the plants. Higher concentrations in the roots is justified by the role of the root hairs as the first pathway for the uptake of nutrients from the growth media. All sizes used for this study should theoretically be able to be absorbed in the roots of the garden cress plant. Upon calculating the amount of Fe in each IONP-EDTA sample (Table S1), we could deduce that the plants incubated with the $IONP_{20}$-EDTA sample should have an overall larger amount of total Fe content compared to the plants treated with $IONP_{10}$-EDTA sample, which is reflected in the MPS and AAS data collected in Fig. 9b. Nanoparticles may enter the plant through their pores,[67] driven by the recognition of the chelating ligand EDTA, osmotic pressure, and capillary forces. The results showed similar trends of translocation of IONPs in the leaves, stem, and roots indicating translocation of both kinds of particle treatments to aerial parts of the plant in which pore sizes decrease to a range closer to ~20 nm.[67] TEM images and elemental analysis shown in Fig. 9c confirm the translocation of the $IONP_{20}$-EDTA to the leaves. The TEM images show the presence of IONP mostly in the cell wall, which suggests a predominant uptake and translocation of IONP through an apoplastic pathway.[12] In addition, the effective translocation of $IONP_{20}$-EDTA all the way to the leaves of the garden cress plant can be confirmed from the observed magnetic response of the incubated plant to an external bar magnet as demonstrated in the accompanying video†.

Conclusions

In summary, this work reports the effects of IONP-EDTA on the phenotypic characteristics of garden cress plants, showing enhancement in biomass and chlorophyll production. The results show IONP-EDTA as a promising Fe fertilizer to treat chlorosis and fortify plants with nutritional value. Moreover, we demonstrated that MPS can be used for the reliable quantitative analysis of magnetic nanoparticle root accumulation and plant uptake in plant systems, with minimal and non-destructive sample preparation.

Experimental

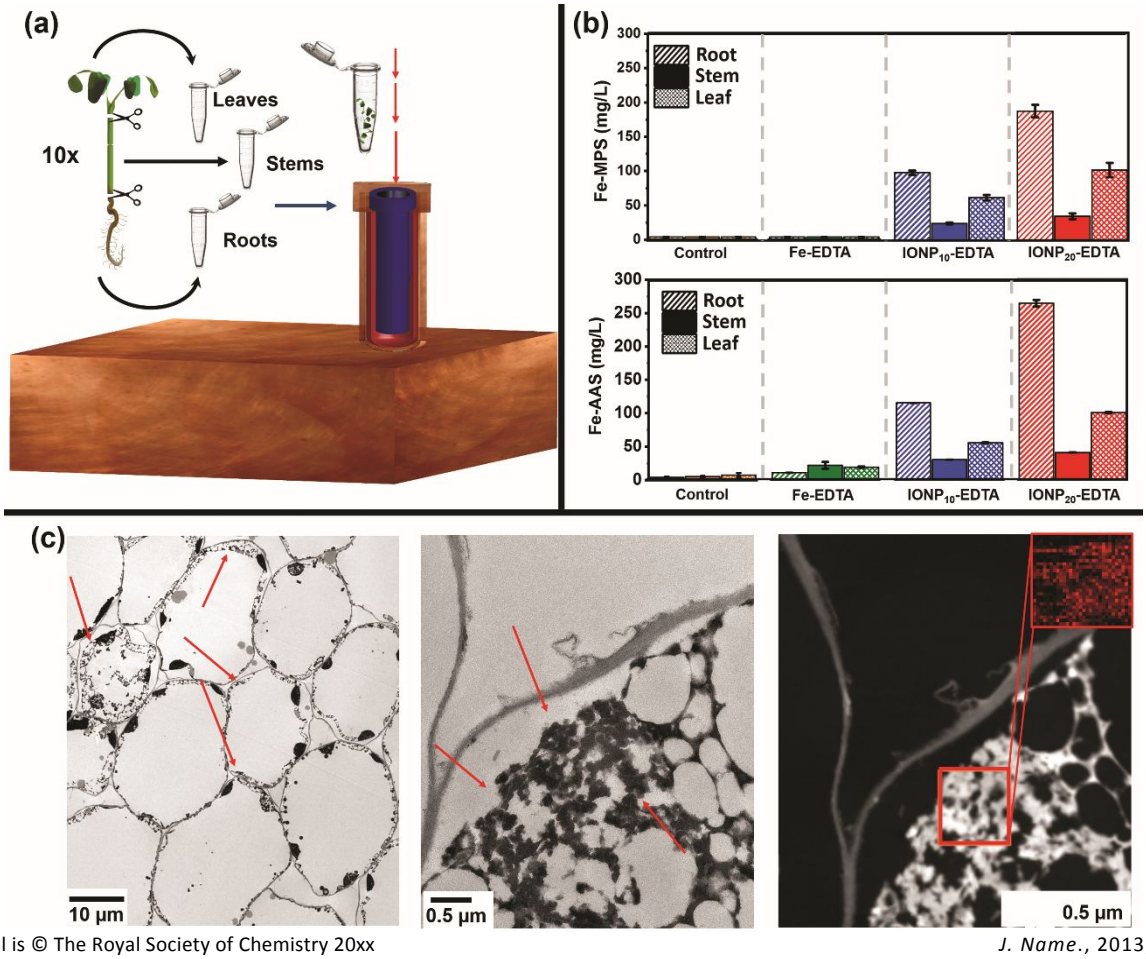

Fig. 9 Translocation studies of $IONP_{10}$-EDTA and $IONP_{20}$-EDTA in garden cress plants: (a) schematic representation of the sample preparation for the measurement of the MPS signal in each plant component; (b) determination of Fe concentration in each component of the plant by MPS and AAS methods with n=50; (c) TEM images of cross-sectional regions of a garden cress leaf from a plant exposed to $IONP_{20}$-EDTA, the red arrows point to the IONP and the red box represents the elemental analysis of the selected area, which shows high concentrations of Fe.

Materials

Iron (III) chloride hexahydrate (98%), anhydrous iron (II) chloride (98%), oleic acid (90%), 1-octadecene (90%), trimethylamine (99%), toluene (HPLC grade, 99%), and ethanol (HPLC grade, 90%) were purchased from Sigma Aldrich (Milwaukee, WI, USA). Ammonium hydroxide (14.8 M), hydrochloric acid (37%), and the iron reference standard solution (1000 mg/L) for the atomic absorption spectroscopic analyses were purchased from Fischer Scientific (Pittsburgh, PA, USA).

N-(trimethoxysilylpropyl)ethylenediaminetriacetate, trisodium salt, 35% in water was purchased from Gelest (Morrisville, PA, USA). EDTA-chelated iron (Fe-EDTA, 13.20%) was purchased from Greenway, Biotech Inc. All of the chemicals and reagents were used as-received. The LED lamp (18 W) dual head plant growth light with LED colors red (660 nm, 24 pcs) and blue (460 nm, 12 pcs) was obtained from LEDMEI (Pembroke, NC, USA). The garden cress seeds were purchased from The Sprout House (Lake Katrine, NY, USA).

Synthesis of iron oxide nanoparticles (IONPs)

Spherical monodisperse oleic acid (OA) capped IONPs were synthesized by a thermal decomposition method.[48,49] The synthesis involves a two-step process: the thermal decomposition of iron oleate to wüstite phase (FeO) nanoparticles and a later mild oxidation step that gives rise to the magnetite (Fe_3O_4) phase. For the formation of the wüstite nanoparticles, the synthesis parameters were controlled in order to produce samples with 10 nm and 20 nm average diameters. For the synthesis of the 10 nm nanoparticles, iron oleate (5.8 mmol), oleic acid (3.2 mmol), and 18 mL of 1-octadecene were mixed in a 25 mL three-neck round bottom flask. The reaction mixture was heated following a rate of 3 ^{o}C/m until it reached a reflux temperature of 320 ^{o}C, whereby the reaction mixture was left to reflux for 1 h. The final product was left to cool at room temperature and collected by centrifugation (7000 rpm, 20 min). For the 20 nm nanoparticles, 12.7 mmol of oleic acid and 10 mL of 1-octadecene were used.

For the second step, the wüstite nanoparticles (1.67 mmol) were oxidized by mixing oleic acid (1.52 mmol), 20 mL 1-octadecene and 10 mg of trimethylamine *N*-oxide (oxidizing agent). The mixture was left to react under constant stirring for 2 h at 130 ^{o}C, followed by reflux at 260 ^{o}C for 1 h. The resultant $IONP_{10}$-OA and $IONP_{20}$-OA samples were isolated by the addition of 1:1 ethanol: toluene solvent mixture (30 mL) and subsequently centrifuged at 7000 rpm for 20 min.

Surface functionalization of IONP with silane-EDTA

The IONPs (4 mM, 4 mL) were mixed with a solution of ammonium hydroxide (NH_4OH) in 1-butanol (1 M, 4 mL), triethylamine (1.4 mL), deionized water (0.5 mL), and *N*-(trimethoxysilylpropyl)ethylenediaminetriacetate (TMS-EDTA) (100 µL) in a 20 mL glass vial. The mixture was left to react for 1 h in a homogenizer (7000 rpm). The resulting product was centrifuged at 7000 rpm for 20 min and the supernatant was removed and the particles were re-dispersed in deionized water.

Materials Characterization

A FEI Tecnai G2 Spirit BioTWIN transmission electron microscope operated at 120 kV was used to evaluate the IONP size and morphology. TEM samples were prepared by adding a drop of the IONP diluted sample on a 50 mesh copper grid and allowed to dry. ImageJ™ software was used to process the TEM data and measure the particle size using an average of 200 nanoparticles. High resolution TEM (200 kV microscope, Tecnai G2 F20) was used to obtain images of the IONP inside of the leaf after fixation. For fixation, the plant sample was first dehydrated in 70 %, 50 % then 30 % ethanol for 5 min each. The sample was then fixed with fixative (2.5 % glutaraldehyde/ 4 % paraformaldehyde in 0.2 M cacodylate buffer) overnight at 4 ^{o}C. The fixation was stopped by washing the sample three times with sodium cacodylate buffer (0.2 M, pH 7.3) for 5 min each wash step. After removal of the buffer solution, post-fixation was done by adding 1 % osmium tetroxide in water and the leaf sample was left for 60 min at 4 ^{o}C. The sample was then washed two times with sodium cacodylate buffer solution (5 min each), rinsed with maleate buffer solution (pH 5.1) once, and stained with 1 % uranyl acetate in maleate buffer for 60 min. Uranyl acetate was then removed by washing the sample with maleate buffer three times. Dehydration was then performed in 30 %, 50 %, 75 %, and 95 % ethanol solution for 20 min each at 4 ^{o}C, followed by dehydration three times for 15 min in 100 % ethanol at room temperature. Dehydration was settled with washing the sample three times with propylene oxide for 15 min each. Propylene oxide was by addition of 1:1 and 1:2 mixtures of propylene oxide/eponate medium at room temperature overnight. The final solution was then changed to pure eponate medium for overnight infiltration at room temperature. On the following day, the sample was polymerized for 24 h for the embedding process.

To be observed in TEM, the embedded sample was cut into sections following two different processes; i) Semi-thin sections of 1 µm were cut with a diamond knife, stained with Toluidin Blue, and then observed with a Leica DM5500 light microscope, and ii) Ultra-thin sections of 85 nm were cut with diamond knife, stained with uranyl acetate and lead citrate, and then observed with a Tecnai G2 SpiritBT, electron microscope operated at 120 kV.

The particle size distribution was analyzed by dynamic light scattering (DLS) on a ZetaPALS particle size analyzer (Brookhaven, Upton, NY, USA) at a scattering angle of 90°. Elemental analyses were performed using atomic absorption spectroscopy (AAS, Varian 220FS AA). The surface functionalization of the IONP was evaluated using attenuated total reflectance-Fourier transform infrared spectroscopy (ATR-FTIR) in a range of 500–4000 cm^{-1} using a Jasco FT/IR-4600 ATR-FTIR spectrometer. The powder X-ray diffractometer (PXRD) patterns of the samples were collected using a Rigaku MiniFlex X-ray powder diffractometer with Cu Kα radiation (λ = 0.154 nm).

Seed Germination and Plant Growth

Garden cress (*Lepidium sativum)* seeds were placed into a plastic container with 4 by 6 pots (2x2 cm). Each pot contained a total of 10 seeds in 3 mL of hydroponic media (volume that was kept throughout the entire growth cycle). The plants were grown at room temperature under red (660 nm, 24 pcs) and blue (460 nm, 12 pcs) LED light lamp (18 W) irradiation for 12 h. Five days after seedling emergence, samples were treated with a total 500 mg/L of Fe for the various sized IONP-EDTA and left to grow for five more days (total growth cycle of 10 days). Garden cress plants exposed to tap water and EDTA chelated iron (Fe-EDTA, commercial fertilizer) were used as control groups and were grown simultaneously on every trial.

Length and Biomass Determination

At the end of the growth cycle, the plants were harvested and washed with deionized water until all visible traces of IONP sample were detached from the surface. The plants were stretched, taped, and measured for the length evaluation. The different plant components (leaves, stems, and roots) were separated for further analyses. The separated plant components from each pot (10 plants per pot) were collected and placed in small Eppendorf tubes and dried in a vacuum pump for 4 h. The dried samples were weighed to obtain the biomass. After this step, the plant samples were used in the MPS analysis.

Chlorophyll Measurements

For the chlorophyll measurements, an equivalent of 60 leaves (6 leaves per each plant with 10 plants per pot) were taken from sacrificial samples treated with: control, Fe-EDTA, $IONP_{10}$-EDTA and $IONP_{20}$-EDTA. Each separated group of leaves were placed in 5 mL glass vials and weighed by difference. Deionized water was added to each vial, and the samples were boiled for 10 min. After 10 min, the water was removed, ethanol (95%, 3 mL) was added, and the samples were placed in a 50 ^{o}C water bath for approximately 1 h. Complete bleaching of the leaves was observed. Chl_a and Chl_b were separated by using an alumina column with 100 % hexane, 90:10 hexane: acetone, and 80:20 hexane:acetone mobile phases based on a procedure previously reported method.[68] After the chlorophyll extraction, UV-vis absorption measurements were performed.

Magnetic Particle Spectrometry Analysis

To study the absorption of IONPs in garden cress, an MPS analysis of sacrificial hydroponic media was performed for $IONP_{10}$-EDTA and $IONP_{20}$-EDTA. The hydroponic media solution was sacrificed since the first day of incubation with the treatments, till the end of the cycle. Each collected sample was vortex mixed (1200 rpm) for 1 min and then aliquots of 450 µL were collected and placed into small Eppendorf tubes to perform the MPS analysis. The concentrations were calculated by using a calibration curve generated with each particle type ($IONP_{10}$-EDTA and $IONP_{20}$-EDTA) adjusting to the total initial volume. All analyses were performed in triplicate per sample run.

For the study of the translocation of IONPs through the plant components, once the samples were cleaned, separated into leaves, stem, and roots, dried and weighed, MPS measurements were performed. A total of 5 pots were evaluated per sample (control, Fe-EDTA, $IONP_{10}$-EDTA and $IONP_{20}$-EDTA). This equals 50 sets of 6 leaves, 50 stems, and 50 root samples per condition. The concentrations were calculated by using a calibration curve generated for each particle ($IONP_{10}$-EDTA and $IONP_{20}$-EDTA).

Elemental Analysis Using Atomic Absorption Spectroscopy (AAS)

Samples used for the AAS analysis, were finely ground in a tissue grinder to facilitate the digestion of the sample. For total leaf, stem, and root Fe concentration, the samples were acid-digested at 150 ^{o}C for 12 h in a Teflon lined vessel with 3 mL of 70 % nitric acid. Finally, the samples were diluted with ICP water to 20 mL and analyzed for Fe using flame AAS.

Statistical Analysis

All of the experimental results were evaluated using an analysis of variance (ANOVA). The data was examined using Microsoft Excel and Origin. Significance was tested as compared between all different treatments with a $p < 0.05$.

Conflicts of interest

Authors declare no competing financial interest.

Acknowledgements

ACSS, MJ, MNL, SW, and NBM were supported by a NSF-CAREER Grant (DMR-1253358) from the Solid State and Materials Chemistry Program. We also thank Prof. Ijiri from the Department of Physics at Oberlin College for access to the VSM that was purchased through funds from NSF (DUE-9950606), and Dr. Gao for the HRTEM measurement that was obtained at the TEM facility at the Liquid Crystal Institute, Kent State University, supported by the Ohio Research Scholars Program Research Cluster on Surfaces in Advanced Materials.

References

1 W. M. Stewart, D. W. Dibb, A. E. Johnston and T. J. Smyth, *Agron. J.*, 2005, **97**, 1–6.
2 S. Zhang, N. Gao, T. Shen, Y. Yang, B. Gao, Y. C. Li and Y. Wan, *J. Mater. Chem. A*, 2019, **7**, 9503.
3 W. Li and P. Lan, *Front. Plant Sci.*, 2017, **8**, 40.
4 M. Tagliavini, J. Abadía, A. D. Rombolà, A. Abadía, C. Tsipouridis and B. Marangoni, *J. Plant Nutr.*, 2000, **23**, 2007–2022.
5 K. L. Straub, M. Benz and B. Schink, *FEMS Microbiol. Ecol.*, 2001, **34**, 181–186.
6 J. Morrissey and M. L. Guerinot, *Chem. Rev.*, 2009, **109**, 4553–4567.
7 M. Takahashi, H. Nakanishi, S. Kawasaki, N. K. Nishizawa and S. Mori, *Nat. Biotechnol.*, 2001, **19**, 466–469.

8 J. Abadía, S. Vázquez, R. Rellán-Álvarez, H. El-Jendoubi, A. Abadía, A. Alvarez-Fernández and A. F. López-Millán, *Plant Physiol. Biochem*., 2011, **49**, 471–482.
9 C. Surridge, *Nature*, 2004, **428**, 630–631.
10 I. Orera, J. A. Rodríguez-Castrillón, M. Moldovan, J. I. García-Alonso, A. Abadía, J. Abadía and A. Álvarez-Fernández, *Metallomics*, 2010, **2**, 646–657.
11 T. C. Hutchinson, *Nature*, 1967, **214**, 943–945.
12 R. A. Sperotto, F. K. Ricachenevsky, V. de Abreu Waldow and J. P. Fett, *Plant Sci.*, 2012, **190**, 24–39.
13 H. Marschner and V. Römheld, *Plant Soil*, 1994, **165**, 261–274.
14 C. A. Krohling, F. J. Eutrópio, A. A. Bertolazi, L. B. Dobbss, E. Campostrini, T. Dias and A. C. Ramos, *J. Soil Sci. Plant Nutr*., 2016, **62**, 39–47.
15 S. Santi and W. Schmidt, *New Phytol*., 2009, **183**, 1072–1084.
16 N. J. Robinson, C. M. Procter, E. L. Connolly and M. L. Guerinot, *Nature*, 1999, **397**, 694–697.
17 R. J. DiDonato Jr, L. A. Roberts, T. Sanderson, R. B. Eisley and E. L. Walker, *The Plant J.*, 2004, **39**, 403-414.
18 S. Thomine and G. Vert, *Curr. Opin. Plant Biol*., 2013, **16**, 322–327.
19 A. R. Meda, E. B. Scheuermann, U. E. Prechsl, B. Erenoglu, G. Schaaf, H. Hayen, G. Weber and N. von Wirén, *Plant Physiol*., 2007, **143**, 1761–1773.
20 C. Pineau, S. Loubet, C. Lefoulon, C. Chalies, C. Fizames, B. Lacombe, M. Ferrand, O. Loudet, P. Berthomieu and O. Richard, *PLoS Genet*., 2012, **8**, e1003120.
21 A. Lešková, R. F. H. Giehl, A. Hartmann, A. Fargašová and N. von Wirén, *Plant Physiol*., 2017, **174**, 1648–1668.
22 N. von Wirén, H. Khodr and R. C. Hider, *Plant Physiol.,* 2000, **124**, 1149-1158.
23 S. López-Rayo, D. Hernández and J. J. Lucena, *J. Agric. Food Chem*., 2009, **57**, 8504–8513.
24 G. R. Rout and S. Sahoo, *Rev. Agric. Sci*., 2015, **3**, 1–24.
25 A. Singh, N. B. Singh, I. Hussain, H. Singh and S. C. Singh, *Adv. Exp. Med. Biol*., 2015, **4**, 25–40.
26 R. G. Cantera, A. M. Zamarreño and J. M. García-Mina, *J. Agric. Food Chem*., 2002, **50**, 7609–7615.
27 H. Tombuloglu, Y. Slimani, H. Güngüneş, G. Tombuloglu, M. A. Almessiere, H. Sozeri, A. Baykal and I. Ercan, *J. Supercond. Novel Magn.*, 2019, 1-10.
28 R. Sheykhbaglou, M. Sedghi, M. T. Shishvan and R. S. Sharifi, *Not. Sci. Biol*., 2010, **2**, 112–113.
29 H. Tombuloglu, Y. Slimani, G. Tombuloglu, A. D. Korkmaz, A. Baykal, M. Almessiere and I. Ercan*, Plant Physiol. Biochem.*, 2019, **139**, 56-65.
30 H. Tombuloglu, Y. Slimani, G. Tombuloglu, M. Almessiere and A. Baykal, *Chemosphere,* 2019, **226**, 110-122.
31 S. Dhoke, P. Mahajan, R. Kamble and A. Khanna, *Nanotechnol. Dev.*, 2013, **3**, e1.
32 S. Bombin, M. LeFebvre, J. Sherwood, Y. Xu, Y. Bao and K. M. Ramonell, *Int. J. Mol. Sci*., 2015, **16**, 24174–24193.
33 Y. Marusenko, J. Shipp, G. A. Hamilton, J. L. L. Morgan, M. Keebaugh, H. Hill, A. Dutta, X. Zhuo, N. Upadhyay, J. Hutchings, P. Herckes, A. D. Anbar, E. Shock and H. E. Hartnett, *Environ. Pollut*., 2013, **174**, 150–156.
34 H. Zhu, J. Han, J. Q. Xiao and Y. J. Jin, *J. Environ. Monit*., 2008, **10**, 713–717.
35 M. Rui, C. Ma, Y. Hao, J. Guo, Y. Rui, X. Tang, Q. Zhao, X. Fan, Z. Zhang, T. Hou and S. Zhu, *Front. Plant Sci*., 2016, **7**, 1–10.
36 I. S. Ahmadov, M. A. Ramazanov, A. Sienkiewicz and L. Forro, *Dig. J. Nanomater. Biostruct*., 2014, **9**, 1149–1157.
37 A. Tomitaka, H. Arami, S. Gandhi and K. M. Krishnan, *Nanoscale*, 2015, **7**, 16890-16898.
38 T. Knopp, N. Gdaniec and M. Möddel, *Phys. Med. Biol*., 2017, **62**, R124.
39 B. Gleich and J. Weizenecker, *Nature*, 2005, **435**, 1214–1217.
40 A. Malhotra and T. M. Buzug, *Curr. Dir. Biomed. Eng*., 2018, **4**, 83–86.
41 L. M. Bauer, S. F. Situ, M. A. Griswold and A. C. S. Samia, *J. Phys. Chem. Lett*., 2015, **6**, 2509–2517.
42 R. M. Ferguson, A. P. Khandhar, C. Jonasson, J. Blomgren, C. Johansson and K. M. Krishnan, *IEEE Trans. Magn.,* 2013, **49**, 3441-3444.
43 A. Rauwerdink, A. Giustini and J. Weaver, *Nanotechnology*, 2010, **21**, 455101.
44 P. W. Goodwill, E. U. Saritas, L. R. Croft, T. N. Kim, K. M. Krishnan, D. V. Schaffer and S. M. Conolly, *Adv. Mater*., 2012, **24**, 3870–3877.
45 J. Li, J. Hu, C. Ma, Y. Wang, C. Wu, J. Huang and B. Xing, *Chemosphere*, 2016, **159**, 326–334.
46 J. Yuan, Y. Chen, H. Li, J. Lu, H. Zhao, M. Liu, G. S. Nechitaylo and N. N. Glushchenko, *Sci. Rep*., 2018, **8**, 3228.
47 K. Morris, A. Linkies, K. Müller, K. Oracz, X. Wang, J. R. Lynn, G. Leubner-Metzger and W. E. Finch-Savage, *Plant Physiol.*, 2011, **155**, 1851-1870.
48 J. Park, K. An, Y. Hwang, J. Park, H. Noh, J. Kim, J. Park, N. Hwang and T. Hyeon, *Nat. Mater*., 2004, **3**, 891–895.
49 D. J. Burke, N. Pietrasiak, S. F. Situ, E. C. Abenojar, M. Porche, P. Kraj, Y. Lakliang and A. C. S. Samia, *Int. J. Mol. Sci*., 2015, **16**, 23630–23650.
50 K. Shawle, M. Urge and G. Animut, *SpringerPlus*, 2016, **5**, 1441.
51 G. L. Barbosa, F. D. A. Gadelha, N. Kublik, A. Proctor, L. Reichelm, E. Wissinger, G. M. Wohlleb and R. U. Halden*, Int. J. Environ. Res. Public Health*, 2015, **12**, 6879–6891.
52 A. F. López-Millán, D. Duy and K. Philippar, *Front. Plant. Sci*., 2016, **7**, 178.
53 M. O. Senge, A. A. Ryan, K. A. Letchford, S. A. MacGowan and T. Mielke, *Symmetry*, 2014, **6**, 781–843.
54 J. Balk and S. Lobréaux, *Trends Plant Sci*., 2005, **10**, 1360–1385.
55 M. U. F. Kirschbaum, *Plant Physiol*., 2011, **155**, 117–124.
56 L. M. Bauer, D. W. Hensley, B. Zheng, Z. W. Tay, P. W. Goodwill, M. A. Griswold and S. M. Conolly, *Rev. Sci. Instrum*., 2016, **87**, 055109.
57 L. M. Bauer, S. F. Situ, M. Griswold and A. C. S. Samia, *Nanoscale*, 2016, **8**, 12162–12169.
58 P. W. Goodwill, K. Lu, B. Zheng and S. M. Conolly, *Rev. Sci. Instrum*., 2012, **83**, 033708.
59 P. W. Goodwill and S. M. Conolly, *IEEE T. Med. Imaging,* 2011, **30**, 1581–1590.
60 H. Arami and K. M. Krishnan, *J. Appl. Phys*., 2014, **7**, 17B306.
61 A. Lak, M. Cassani, B. T. Mai, N. Winckelmans, D. Cabrera, E. Sadrollahi, S. Marras, H. Remmer, S. Fiorito, L. Cremades-Jimeno, F. J. Litterst, F. Ludwig, L. Manna, F. J. Teran, S. Bals and T. Pellegrino, *Nano Lett.,* 2018, **18**, 6856–6866.
62 R. M. Ferguson, A. P. Khandhar, S. J. Kemp, H. Arami, E. U. Saritas, L. R. Croft, J. Konkle, P. W. Goodwill, A. Halkola, J. Rahmer, J. Borgert, S. M. Conolly and K. M. Krishnan, *IEEE T. Med. Imaging,* 2015, **34**, 1077-1084.
63 I. M. Perreard, D. B. Reeves, X. Zhang, E. Kuehlert, E. Forauer and J. B. Weaver, *Phys. Med. Biol*., 2014, **59**, 1109–1119.
64 J. Xie and S. Jon, *Theranostics*, 2012, **2**, 122–124.
65 T. P. Durrett., W. Gassmann and E. E. Rogers, *Plant Physiol.,* 2007, **144**, 197-205.
66 J. Narayanan, J. Y. Xiong and X. Y. Liu, *J. Phys.: Conf. Ser.,* 2006, **28**, 83.
67 P. Wang, E. Lombi, F. Zhao and P. M. Kopittke, *Trends Plant Sci.*, 2016, **21**, 699–712.
68 A. Johnston, J. Scaggs, C. Mallory, A. Haskett. D. Warner, E. Brown, K. Hammond, M. M. McCormick and O. M. McDougal, *J. Chem. Educ.,* 2013, **90**, 796–798.

Table of Contents Entry

Magnetic particle spectroscopy offers a reliable and facile approach for the screening of promising nanoengineered fertilizers.